Supplementary information file for the article: Study of a phosphorescent cationic iridium(III) complex displaying blue shift in crystals

Emiliano Martínez-Vollbert,[a] Christian Philouze,[a] Isabelle Gautier-Luneau,[b] Yohann Moreau,[c] Pierre-Henri Lanoë,[a]* and Frédérique Loiseau[a]*

[a] Univ. Grenoble Alpes, CNRS, DCM, 38000 Grenoble, France
[b] Univ. Grenoble Alpes, CNRS, Grenoble INP, Institut Néel, 38000 Grenoble, France
[c] Univ. Grenoble Alpes, CEA, CNRS, IRIG, CBM, F-38000 Grenoble, France
* Correspondence pierre-henri.lanoe@univ-grenoble-alpes.fr ; Frederique.loiseau@univ-grenoble-alpes.fr

Table of contents

General considerations 2
Crystal Structure Determinations and Refinements 2
Synthesis 4
TD-DFT calculation of the absorption spectrum of complex A, singlet ground state, optimized in CH_2Cl_2. 10
DFT calculation on orbitals localization for the radiative transition $T_1 \rightarrow S_0$ 14
Figure S 1: Views (from top to bottom: projection in bc, ac, and ab planes) of the crystal packing with the counter ions in space filling. Hydrogens atoms have been omitted for clarity. 6
Figure S 2: Packing of the molecules in ball and sticks, along the a axis. Hydrogens atoms have been omitted for clarity. 7
Figure S 3: Projection of the chains in ab plane 7
Figure S 4: View of the chains along the direction ac. 8
Figure S 5: Intracatenar Hydrogen bond between the H22 atoms and the C11-C12 carbon bond. 8
Figure S 6: Intramolecular interaction between the hydrogen atom H9 and the nitrogen atom N3. 9
Figure S 7: Powder X-ray diffraction diagram of crystals (black) registrated at room temperature compared to calculated pattern from crystal structure (200 K) (red). 9
Figure S 8: Luminescence decays. 10
Figure S 9: Reconstructed UV-Vis absorption spectrum for complex A only, in chloromethane (right scale: Molar absorbance computed as detailed in https://gaussian.com/uvvisplot/), together with computed peaks (left scale, arbitrary units for oscillator strength). Results from TD-DFT calculations, MN15/Def2SVP, CH_2Cl_2 implicit solvent. 12
Figure S 10: Natural transition Orbitals (Hole/Electron) for the four lowest energetic transitions. TD-DFT MN15/Def2-SVP, implicit solvent model for CH_2Cl_2. 13
Figure S 11: Frontier orbitals of Complex **A** in vaccuum: SOMO's of the triplet state (left) and HOMO/LUMO of the singlet state (right). 15
Figure S 12: Frontier orbitals of Complex **A** in CH_sCl_2: SOMO's of the triplet state (left) and HOMO/LUMO of the singlet state (right). 16
Figure S 13: Frontier orbitals of Complex **A** in the crystal: SOMO's of the triplet state (left) and HOMO/LUMO of the singlet state(right). 17
Figure S 14: ^1H NMR spectra of the cyclometallating ligand 400 MHz in $CDCl_3$ 18
Figure S 15: ^{13}C NMR spectra of the cyclometallating ligand 101 MHz in $CDCl_3$. 18
Figure S 16: ^1H NMR spectra of complex **A** 500 MHz in CD_2Cl_2. 19
Figure S 17: ^{13}C NMR spectra of complex **A**, 126 MHz in CD_2Cl_2 19
Figure S 18 : ^{19}F NMR spectra of complex **A** 470 MHz in CD_2Cl_2 20

Figure S 19: ^{31}P NMR spectra of complex **A** 202 MHz in CD_2Cl_2.....20

General considerations

Commercially available reagents were purchased from Sigma-Aldrich®, Alfa Aesar®, Acros Organics®, TCI Chemical®, Merck®, Strem® or Fluorochem® and used as received unless otherwise specified. Solvents were obtained from same commercial sources and used without further purification. For moisture sensitive reactions, glassware was oven-dried prior to use. ^1H NMR spectra were recorded on a 400 MHz and on a 500 MHz in deuterated solvent ($CDCl_3$, DMSO-d^6 or CD_2Cl_2) and data are reported as follows: chemical shift in ppm from tetramethylsilane with solvent as an internal indicator ($CDCl_3$ 7.26 ppm, dmso-d6 2.50 ppm, CD_2Cl_2 5.32 ppm), multiplicity (s = singlet, d = doublet, t = triplet, q = quartet, p = pentet, m = multiplet or overlap of non-equivalent resonances), integration. $^{13}C\{^1H\}$ NMR spectra were recorded either at 101 MHz or at 126 MHz in suitable deuterated solvent and data are reported as follows: chemical shift in ppm from tetramethylsilane with the solvent as an internal indicator ($CDCl_3$ 77.16 ppm, DMSO-d^6 39.52 ppm, CD_2Cl_2 53.84 ppm). $^{19}F\{^1H\}$ NMR spectra were recorded at 376 MHz and at 470 MHz in the suitable deuterated solvent.

Crystal Structure Determinations and Refinements.

An orange plate crystal (0.13 x 0.15 x 0,30 mm) was picked up, coated with a paraffin mixture and mounted with a nylon loop and centered on a Bruker-Nonius diffractometer equipped with an Incoatec high brilliance microsource with multilayers mirrors monochromatized Mo(Kα) radiation (λ = 0.71073 Å) and an APEX II detector. Data collection was made at 200 K with an Oxford Cryosystem cryostream cooler. Final cell parameters were obtained post-refining the whole data. The collected reflections were corrected for Lorentz and polarization effects (EVAL14) and for absorption (SADABS). The resulting data was merged using XPREP. Crystals and data collection details are given in Table S1. Using the OLEX 2[1] analysis package, the crystal structural solution was solved by charge flipping method (Superflip) and refinement was done by full-matrix least squares on F^2 (SHELX2013). C, N, O, F, P, Cl, and Ir atoms were refined anisotropically. H atoms were set geometrically, riding on the carrier atoms, with isotropic thermal parameters. PF_6 anion and dichloroethane molecules displayed disorders which were treated using different positions with partial occupancy rates and restraints.

Table S 1: Crystal data and structure refinement for $[Ir(phbzOMe_2)_2(dmp)PF_6]$.

	$[Ir(phbzOMe_2)_2(dmp)PF_6]$
Empirical formula	$C_{48}\ H_{50}\ Ir\ N_6\ O_4,\ P\ F_6,\ 3(C_2\ H_4\ Cl_2)$
Formula weight/g.mol^{-1}	1408.96
Morphology	plate
Colour	orange
Crystal size/mm	0.13 x 0.15 x 0.30
Crystal system	monoclinic
Space group	C2/c
Temperature/K	200

a/Å	19.554(4)
b/Å	22.055(4)
c/Å	15.394(3)
α/°	90
β/°	117.07(3)
γ/°	90
Volume/Å^3	5911(2)
Z	4
ρ_{calc}/g.cm^{-3}	1.583
μ/mm^{-1}	2.625
F(000)	2832
Radiation/Å	MoKα (λ = 0.71073)
Θ range for data collection/°	2.809 to 30.000
Index ranges	-27 ≤ h ≤ 27, -30 ≤ k ≤ 31, -21 ≤ l ≤ 21
Total reflections	41641
Unique reflections	8603
Observed reflections	3224($F^2 > 2$□)
R*int*	0.0351
Data/restraints/parameters	8603/175/424
Goodness-of-fit on F^2	1.167
Final R indexes [I>=2σ (I)]	R1 = 0.0265, wR2[a] = 0.0644
Final R indexes [all data]	R1 = 0.0362, wR2[a] = 0.0742
Largest diff. peak/hole /e.Å^{-3}	2.163/-1.139

[a] Refinement based on F^2 whith $w = 1/[\sigma^2(Fo)^2 + (0.0278p)^2 + 12.8951p]$ where $p = (Fo^2 + 2Fc^2)/3$

Synthesis

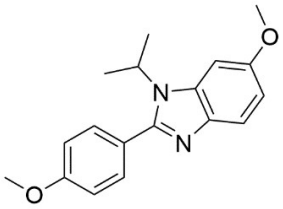

Ligand synthesis

5-methoxy-*N*-(1-methylethyl)-2-nitrobenzenamine (50 mg, 2.4 mmol) and 4-methoxybenzaldehyde (325 mg, 2.4 mmol) were dissolved in a mixture of 2-ethoxyethanol-water 3:1 and heated until dissolution. $Na_2S_2O_4$ (1.25 g, 7.2 mmol) was added to the mixture and refluxed overnight. The reaction mixture was cooled to r. t. and the product extracted with dichloromethane and purified over SiO_2 dichloromethane/pentane (9:1). The title compound was isolated as a white powder (324 mg, 57%).

^{1}H NMR (400 MHz, $CDCl_3$) δ 7.68 (d, *J* = 8.8 Hz, 1H), 7.56 (d, *J* = 8.8 Hz, 1H), 7.07 (d, *J* = 2.3 Hz, 1H), 7.02 (d, *J* = 8.8 Hz, 1H), 6.92 (dd, *J* = 8.8, 2.3 Hz, 1H), 4.78 (hept, *J* = 7.0 Hz, 1H), 3.89 (d, *J* = 9.2 Hz, 6H), 1.62 (d, *J* = 7.0 Hz, 6H). ^{13}C NMR (101 MHz, $CDCl_3$) δ 160.7, 155.9, 153.20, 138.6, 134.2, 130.9, 123.5, 120.5, 114.2, 110.4, 96.9, 56.2, 55.5, 48.7, 21.3. LR-MS (ESI) calcd. for $C_{18}H_{21}N_2O_2$ $[M+H]^+$ 297.38 found 297.07. Elementary analysis calcd. for $C_{18}H_{21}N_2O_2$ C, 72.95; H, 6.80; N, 9.45; found C, 72.70; H, 6.69; N, 9.36.

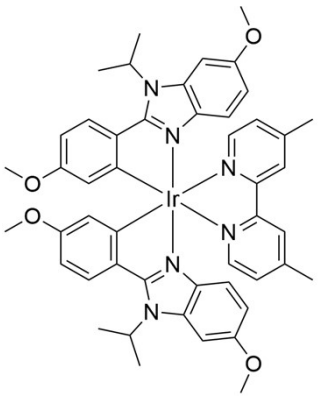

Complex **A**

Following the method first published by Nonoyama,[2] from the ligand, the chloro-bridged Ir(III) dimer was synthesized and used without further purification using $IrCl_3{\cdot}xH_2O$ (60 mg, 0.2 mmol) and 6-methoxy-2-(4-methoxyphenyl)-1-(1-methylethyl)-1*H*-benzimidazole (125 mg, 0.4 mmol) obtaining a yellowish powder (90 mg, 55%). The chloro-bridged dimer (90 g, 0.1 mmol) and 4,4'-dimethyl-2,2'-dipyridyl (20 mg, 0.1 mmol) were dissolved in a mixture CH_2Cl_2-MeOH 1:1 and refluxed overnight. The mixture was cooled to r. t. and reduced to ¼ of the volume, a saturated solution of $KPF_{6(ac)}$ was added until precipitation. The precipitated was filtrated and purified over SiO_2 CH_2Cl_2/acetone (9:1). Complex **A** was isolated as an orange powder (81 mg, 67%). The complex was crystalized by slow vapor diffusion using as solvent 1,2-dichloroethane

and non-solvent diisopropylether obtaining dark orange crystals displaying a green-yellow emission under UV light.

^{1}H NMR (500 MHz, CD_2Cl_2) δ 8.20 (s, 1H), 7.92 (d, *J* = 5.6 Hz, 1H), 7.74 (d, *J* = 8.8 Hz, 1H), 7.25 (dd, *J* = 5.6, 0.9 Hz, 1H), 7.08 (d, *J* = 2.3 Hz, 1H), 6.63 (dd, *J* = 8.8, 2.7 Hz, 1H), 6.54 (dd, *J* = 9.0, 2.3 Hz, 1H), 5.78 (d, *J* = 2.6
(s, 1H), 3.43 (s, 1H), 2.59 (s
163.0, 161.1, 156.9, 156.5,
115.2, 112.4, 108.3, 98.5,
133.9, -137.4, -140.9, -144.
HRMS (ESI) calcd *m/z* 965.
Analysis calcd for $C_{48}H_{50}F_6I$
7.75.

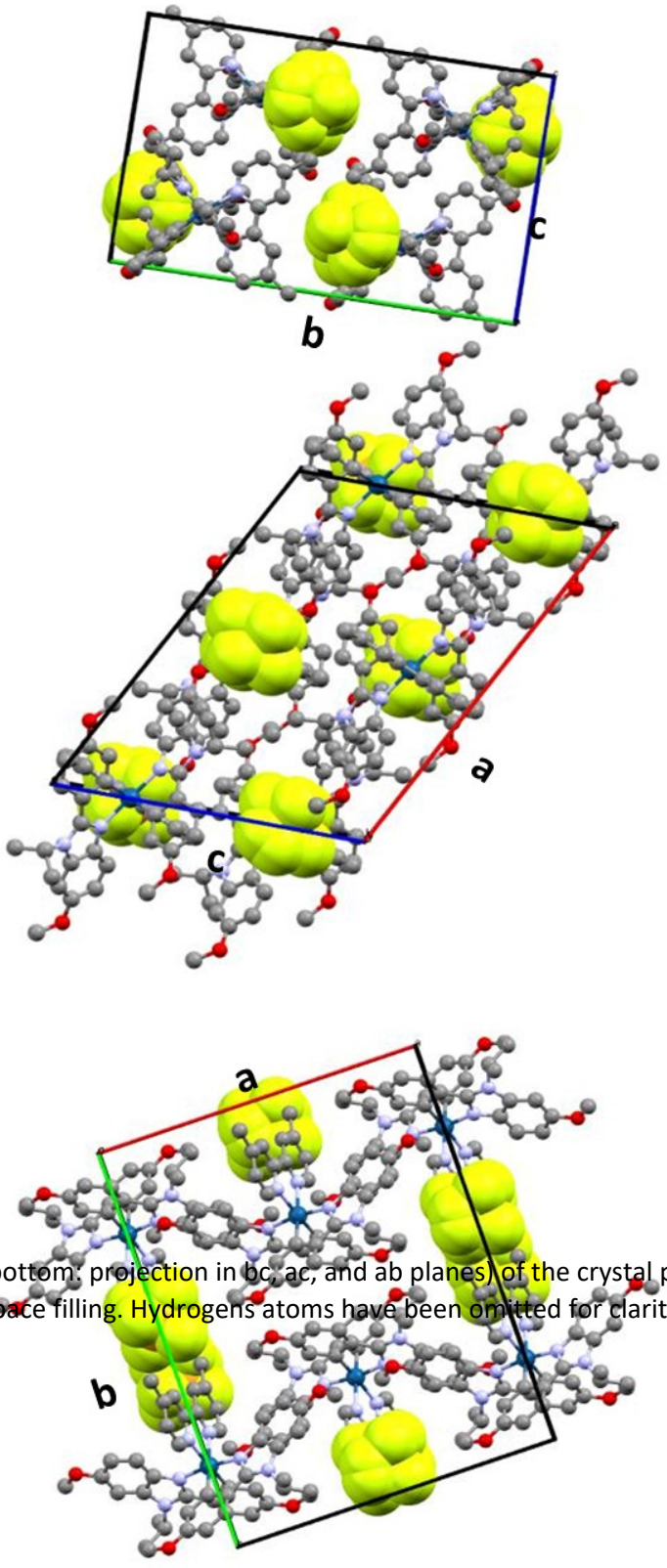

Figure S 1: Views (from top to bottom: projection in bc, ac, and ab planes) of the crystal packing with the counter ions in space filling. Hydrogens atoms have been omitted for clarity.

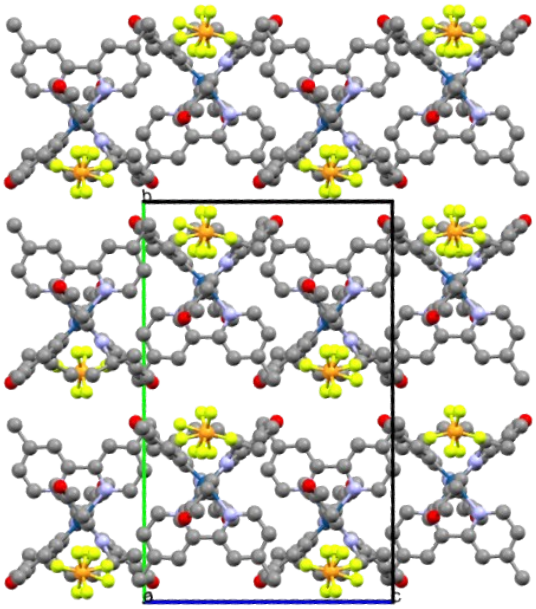

Figure S 2**:** Packing of the molecules in ball and sticks, along the a axis. Hydrogens atoms have been omitted for clarity.

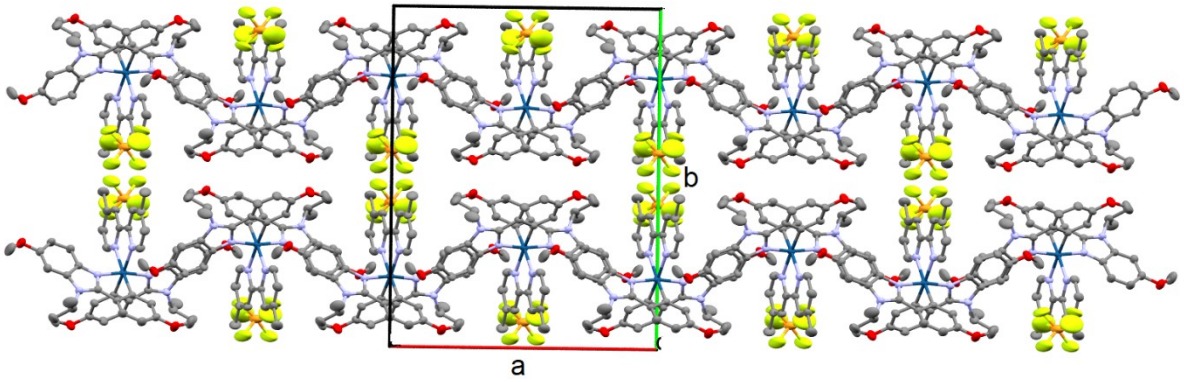

Figure S 3: Projection of the chains in ab plane

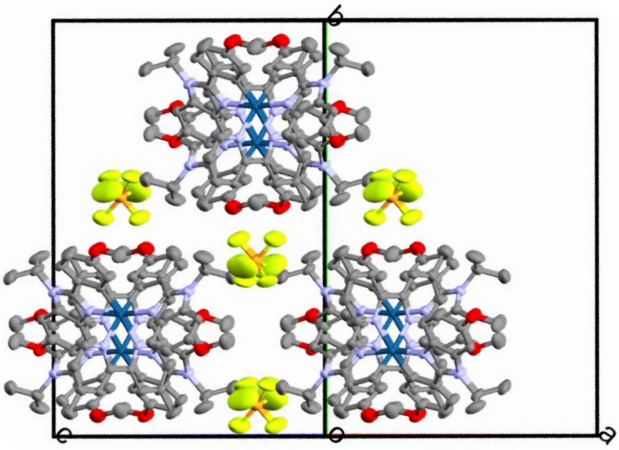

Figure S 4: View of the chains along the direction ac.

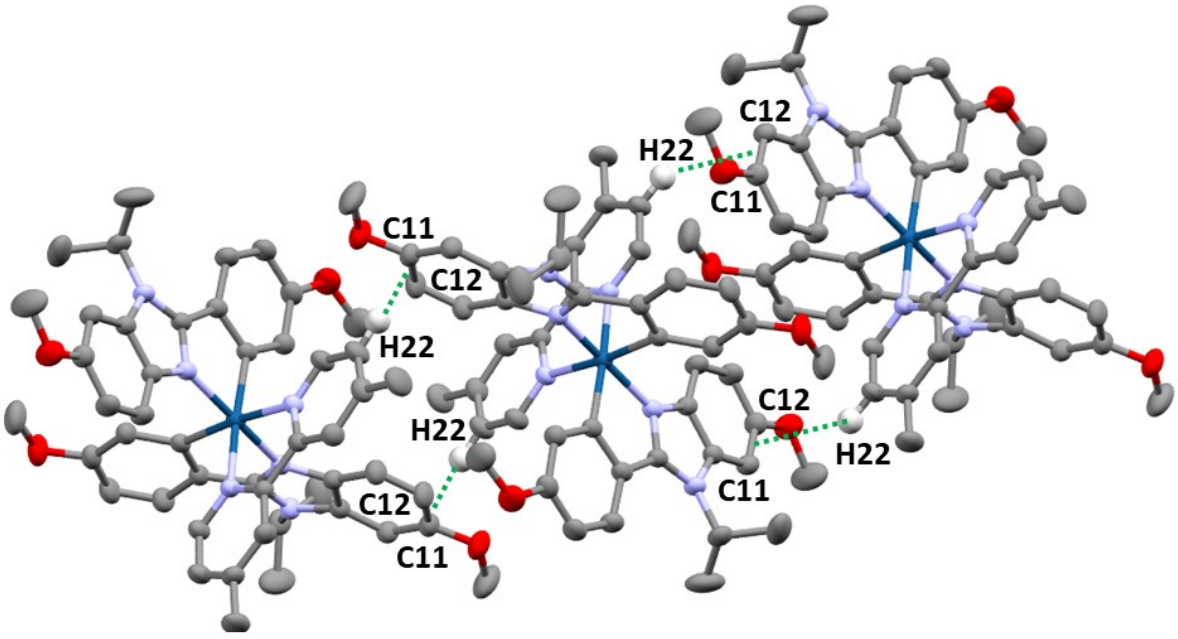

Figure S 5: Intracatenar Hydrogen bond between the H22 atoms and the C11-C12 carbon bond.

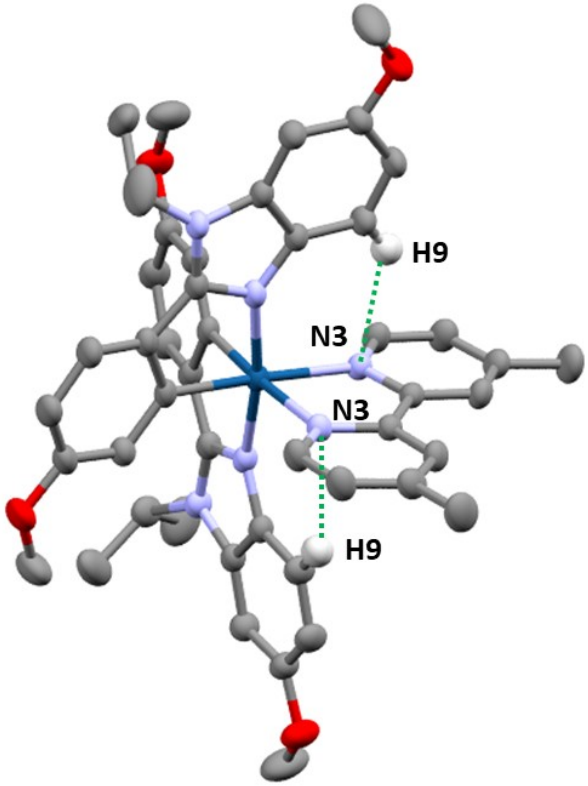

Figure S 6: Intramolecular interaction between the hydrogen atom H9 and the nitrogen atom N3.

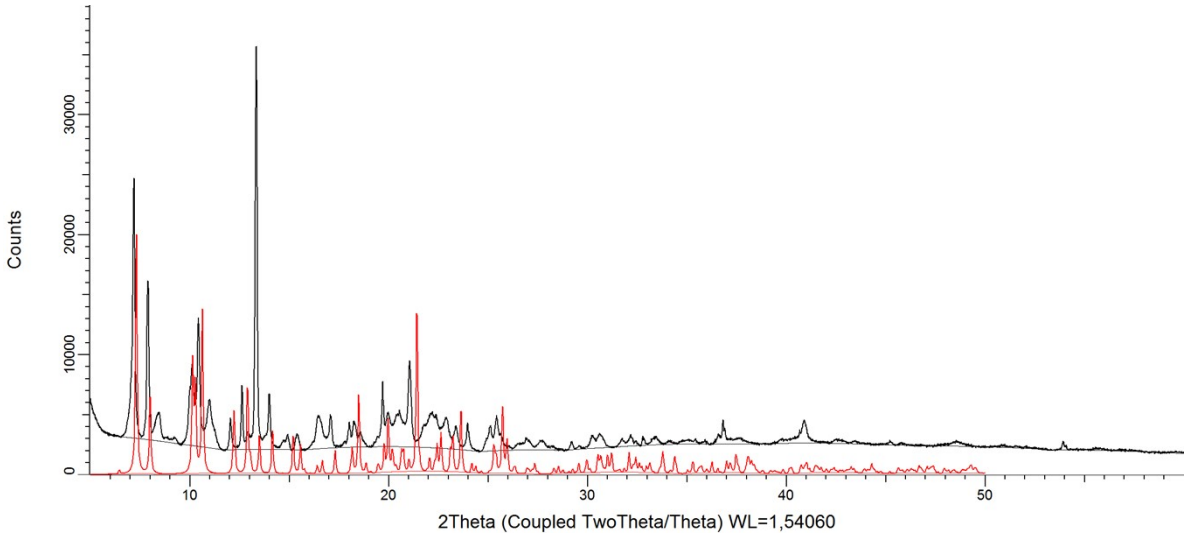

Figure S 7: Powder X-ray diffraction diagram of crystals (black) registrated at room temperature compared to calculated pattern from crystal structure (200 K) (red).

The experimental pattern of crystals (collected indiscriminately from the same batch of crystallization) is similar to calculated one from the crystal structure. The shift of the peaks is due to the measurement realized at different temperatures. Furthermore, PXRD pattern of no grinded crystals shows different intensities due to preferential orientations (002 peak at 2 theta angles = 12.5° for example) and also some additional peaks (with a broadening of the peak at full width at half maximum) probably due to degraded crystals with loss of crystallization solvent. Effectively some unbright crystals are observed under optical microscope. The contribution of this degraded phase is minor.

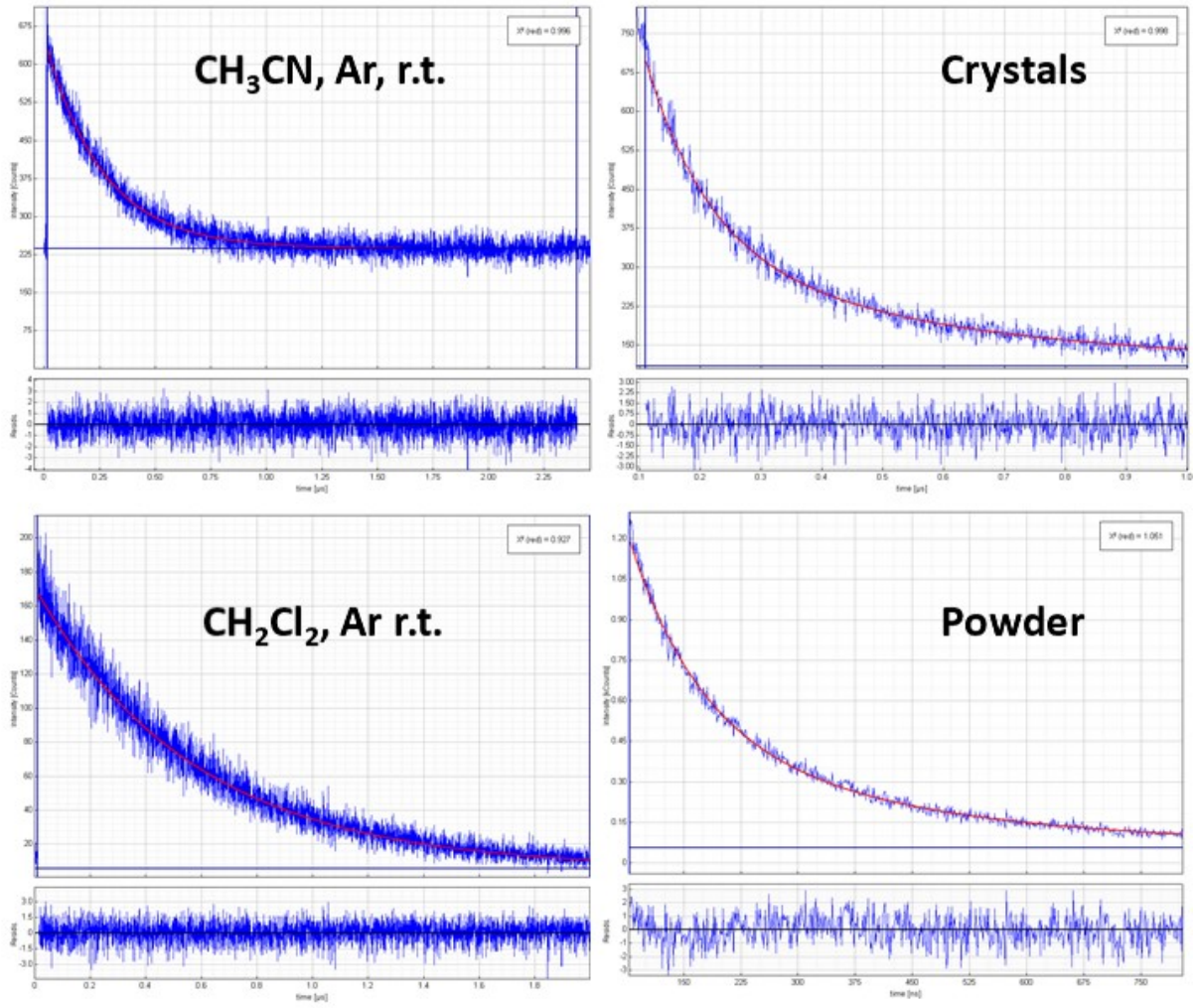

Figure S 8: Luminescence decays.

TD-DFT calculation of the absorption spectrum of complex A, singlet ground state, optimized in CH_2Cl_2.

Table S 2: 20 first absorptions of Complex A in CH_2Cl_2, singlet state, with DE (eV), corresponding l (nm), oscillator strength (noted f) and composition. Orbital nb 214 being the HOMO, and 215 the LUMO.

Transition nb	ΔE (eV)	λ (nm)	Oscillator strength *f*	Composition (occupied OM nb to virtual OM nb, wih weight)
1	3.1018	399.71	0.0004	210 -> 215 0.18286 212 -> 215 0.14841 214 -> 215 0.65573
2	3.2244	384.52	0.0422	211 -> 215 0.19100 213 -> 215 0.67058
3	3.5521	349.04	0.0002	208 -> 215 -0.17532 210 -> 215 -0.30279 212 -> 215 0.59149
4	3.6897	336.02	0.5437	213 -> 218 0.31693 214 -> 216 0.55982

				214 -> 217	-0.16502
5	3.7300	332.39	0.0781	213 -> 216	0.44088
				213 -> 217	-0.12600
				214 -> 218	0.48071
				214 -> 219	0.10587
6	3.8776	319.74	0.0006	206 -> 215	0.10642
				208 -> 215	0.15224
				210 -> 215	0.53154
				212 -> 215	0.31184
				214 -> 215	-0.25173
7	3.9234	316.02	0.1229	205 -> 215	0.12515
				209 -> 215	0.15792
				211 -> 215	0.61351
				213 -> 215	-0.21140
				213 -> 216	0.10793
8	4.0795	303.92	0.0615	211 -> 218	0.19134
				212 -> 216	-0.16182
				213 -> 218	0.49810
				213 -> 221	-0.12999
				214 -> 216	-0.26707
9	4.0857	303.46	0.0269	210 -> 218	-0.14197
				211 -> 216	0.13447
				212 -> 218	-0.14769
				213 -> 216	0.47917
				214 -> 218	-0.39936
10	4.1737	297.06	0.0007	210 -> 215	-0.10307
				210 -> 217	0.14009
				212 -> 217	0.12400
				214 -> 216	0.19186
				214 -> 217	0.62518
11	4.2660	290.64	0.0181	211 -> 217	0.14238
				213 -> 217	0.65453
				214 -> 219	0.11218
12	4.3730	283.52	0.0590	208 -> 216	-0.16703
				210 -> 216	-0.20159
				212 -> 216	0.57106
				212 -> 217	-0.13516
13	4.4018	281.67	0.0004	208 -> 218	0.12217
				210 -> 218	0.22326
				210 -> 219	0.15789
				210 -> 221	-0.11723
				210 -> 227	-0.13982
				212 -> 218	-0.25945
				213 -> 217	-0.11410
				214 -> 218	-0.10743
				214 -> 219	0.36715
				214 -> 221	-0.14359
14	4.4219	280.39	0.1211	204 -> 215	0.28493
				206 -> 215	0.14741
				210 -> 216	0.15072
				211 -> 218	0.15724
				211 -> 219	0.17997
				211 -> 221	-0.12327
				211 -> 227	-0.11596
				212 -> 216	0.11729
				213 -> 218	-0.21822
				213 -> 219	0.30746
				213 -> 221	-0.15054
15	4.4409	279.19	0.0004	203 -> 215	-0.11402
				209 -> 215	0.28162
				210 -> 218	-0.20198
				211 -> 216	-0.13764
				212 -> 218	0.20295
				212 -> 219	0.17956
				214 -> 219	0.41607
16	4.4870	276.32	0.4318	204 -> 215	0.24010
				206 -> 215	0.15389
				209 -> 218	-0.10272
				210 -> 216	-0.26090
				210 -> 217	0.13661

				211 -> 218 -0.27061 212 -> 217 -0.12228 213 -> 219 0.29179 213 -> 221 0.10935
17	4.4917	276.03	0.0327	203 -> 215 -0.19355 205 -> 215 0.12910 207 -> 215 0.13989 209 -> 215 0.44120 211 -> 215 -0.15546 211 -> 216 -0.10387 212 -> 218 -0.25468 214 -> 218 0.10196 214 -> 219 -0.24566
18	4.5196	274.33	0.0414	209 -> 215 0.21988 209 -> 216 0.17059 210 -> 218 0.19087 211 -> 216 0.33482 212 -> 218 0.34394 213 -> 220 -0.13771 214 -> 219 -0.17660
19	4.5620	271.77	0.1574	204 -> 215 -0.34722 206 -> 215 -0.19862 210 -> 216 -0.20835 210 -> 217 -0.13517 212 -> 217 0.13630 213 -> 218 -0.15964 213 -> 219 0.41402
20	4.6231	268.18	0.0279	204 -> 215 -0.10605 206 -> 215 0.11772 208 -> 215 0.60437 210 -> 215 -0.24779

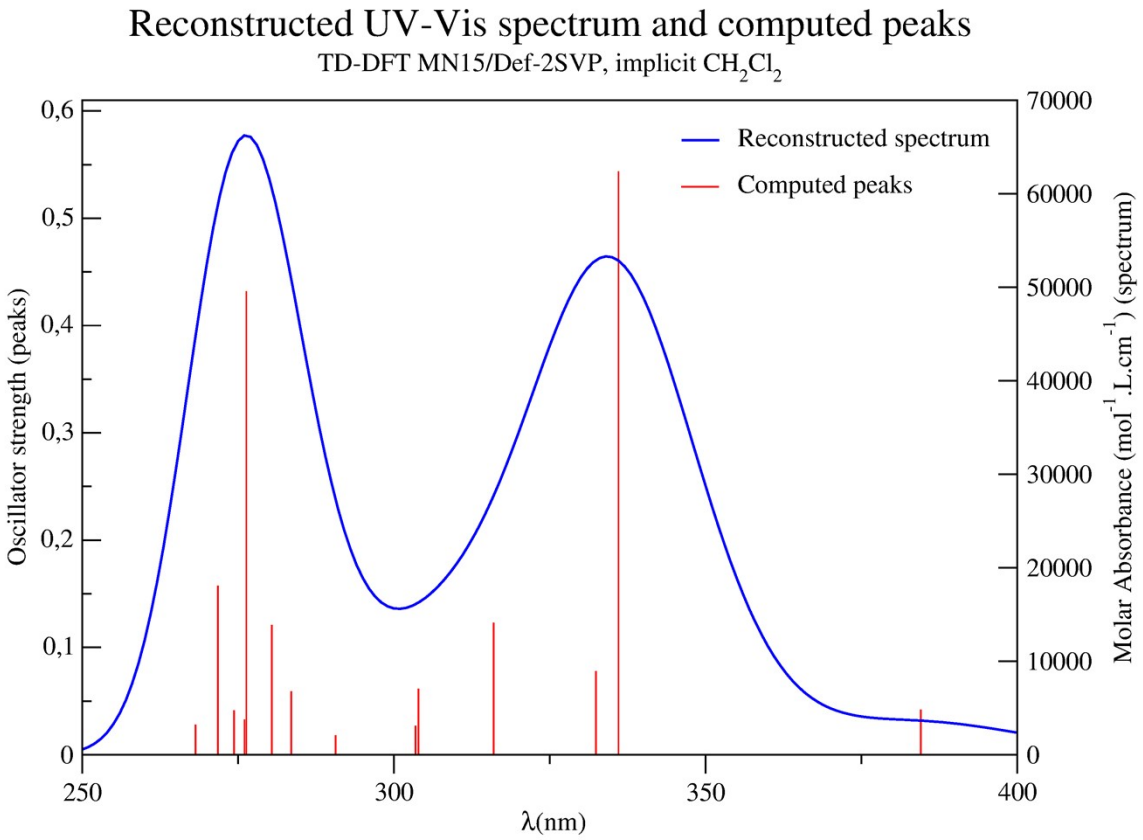

Figure S 9: Reconstructed UV-Vis absorption spectrum for complex A only, in chloromethane (right scale: Molar absorbance computed as detailed in https://gaussian.com/uvvisplot/), together with computed peaks (left scale, arbitrary units for oscillator strength). Results from TD-DFT calculations, MN15/Def2SVP, CH_2Cl_2 implicit solvent.

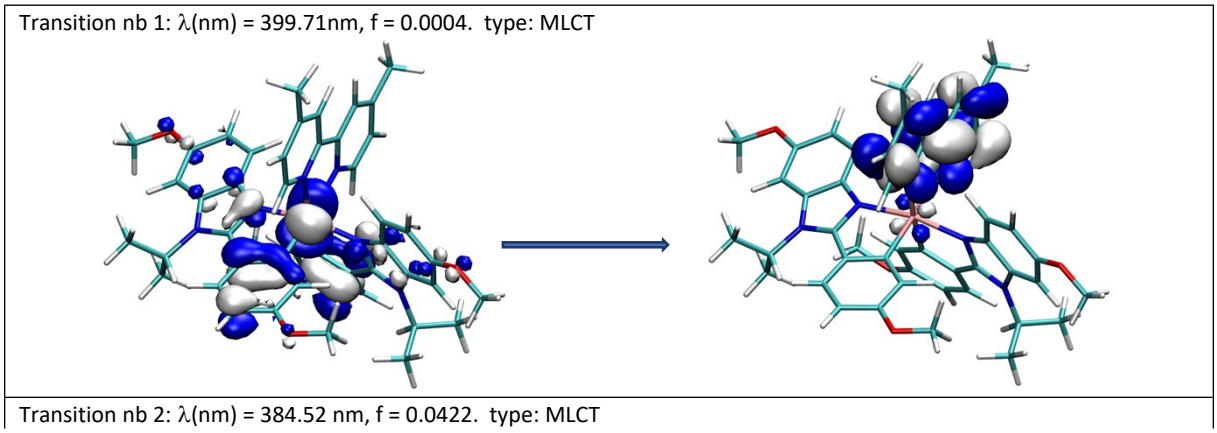

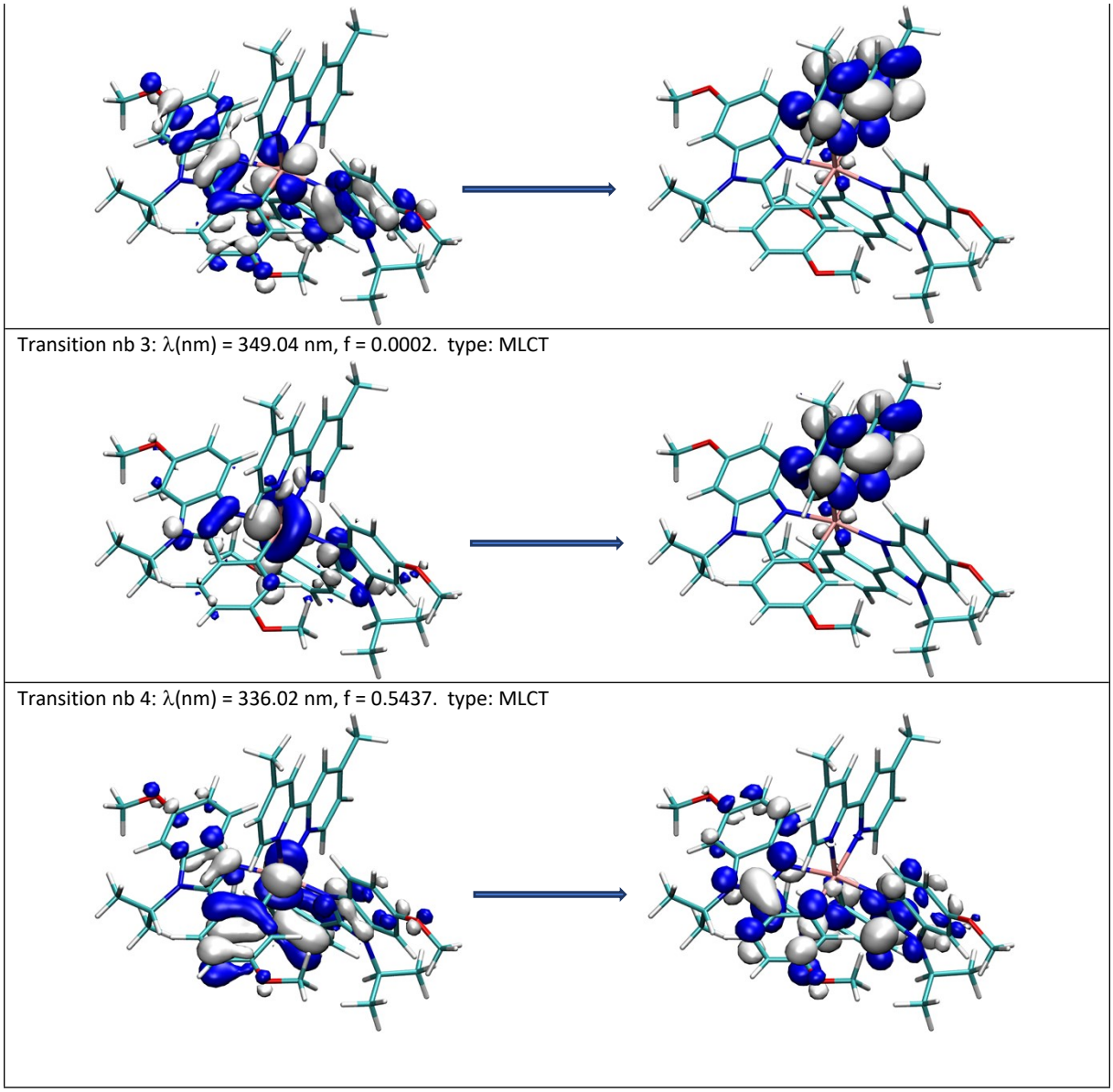

Figure S 10: Natural transition Orbitals (Hole/Electron) for the four lowest energetic transitions. TD-DFT MN15/Def2-SVP, implicit solvent model for CH_2Cl_2.

DFT calculation on orbitals localization for the radiative transition $T_1 \rightarrow S_0$

Kohn-Sham orbitals represented hereafter represent the singly occupied molecular orbitals (SOMO 1 and 2) in the triplet state *vs* the HOMO and LUMO in the singlet state for the three cases: in vacuum, with an implicit solvent model for CH_2Cl_2 and embedded in the model of crystal. For each situation, the optimized geometry of the triplet in the specific condition is used for both triplet and singlet configurations, consistently with the view of a vertical T→S transition.

In the three cases, the emission can be seen as a deexcitation of the electron described by the SOMO 2 orbital of the triplet, located on the dimethylbipyridine (dmp) towards the HOMO of the singlet, delocalized between the metal and the 2-phenylbenzimidazole ligands (pbi)

It is noteworthy that while the SOMO-1 and the HOMO are evenly distributed on the two 2-phenylbenzimidazole ligands in vacuum, it tends to become dissymmetric in solvent and in crystal, with a complete relocalization in some cases. That behavior is consistent with a polarization due to the environment in the two latter cases.

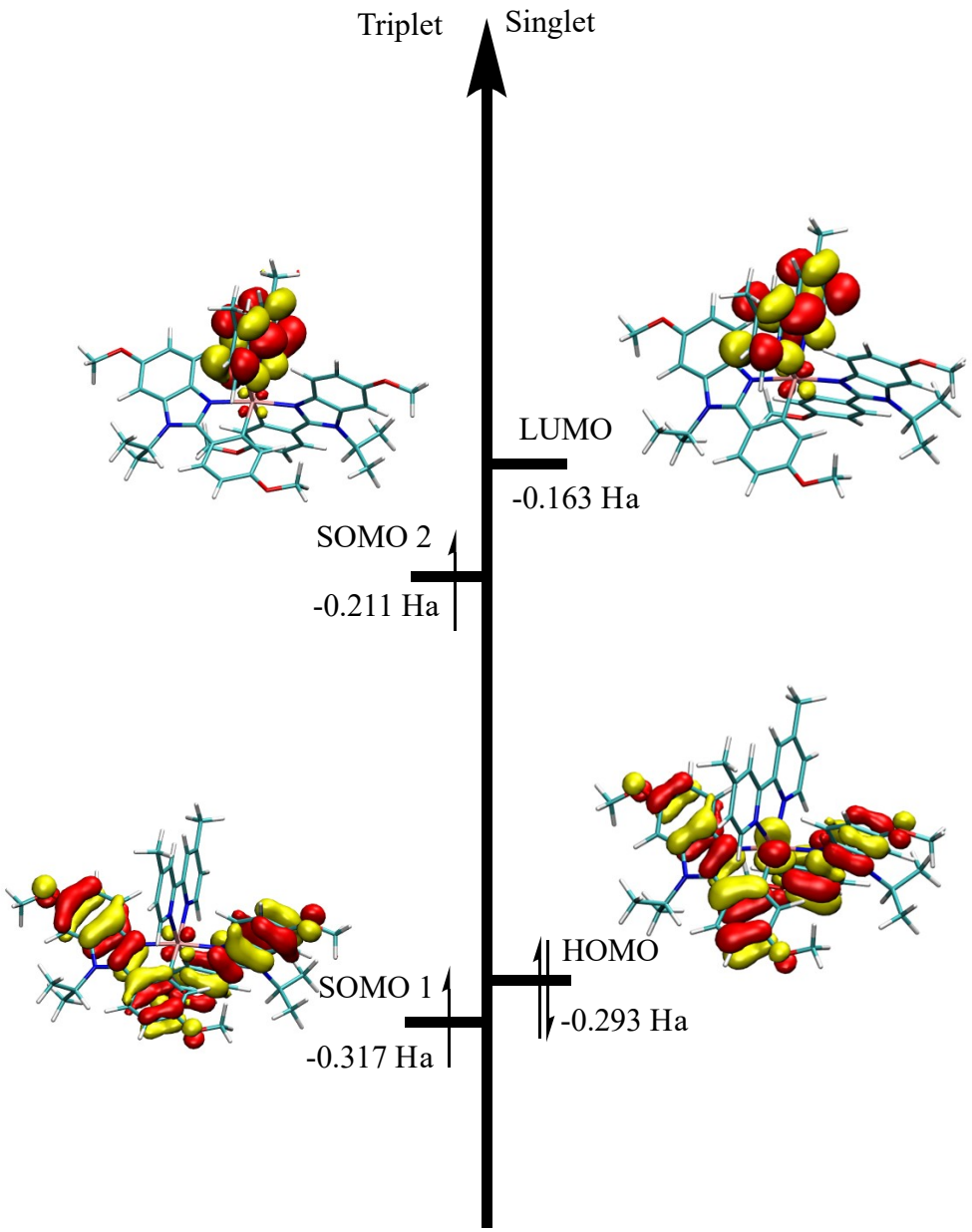

Figure S 11: Frontier orbitals of Complex **A** in vaccuum: SOMO's of the triplet state (left) and HOMO/LUMO of the singlet state (right).

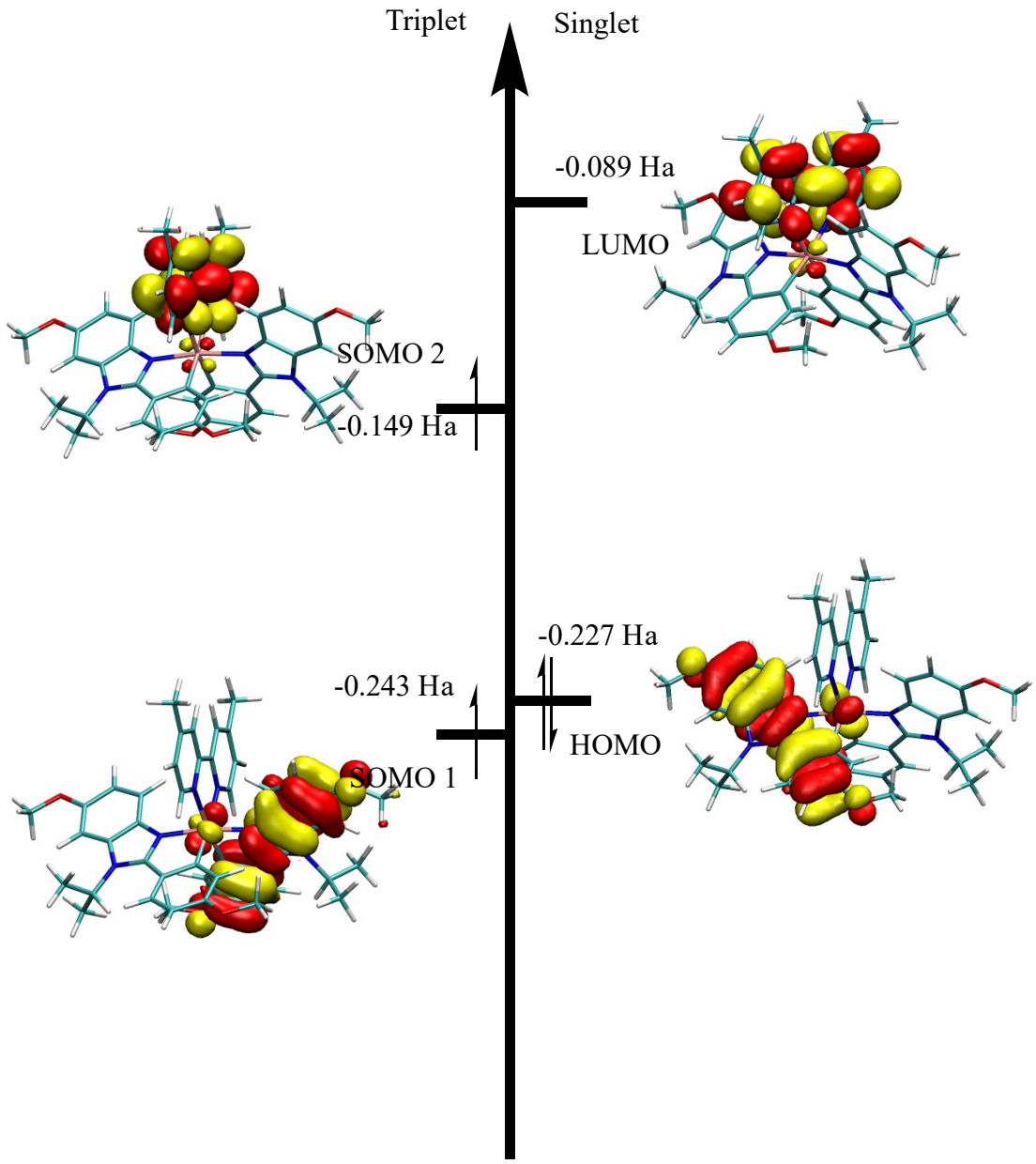

Figure S 12: Frontier orbitals of Complex **A** in CH_sCl_2: SOMO's of the triplet state (left) and HOMO/LUMO of the singlet state (right).

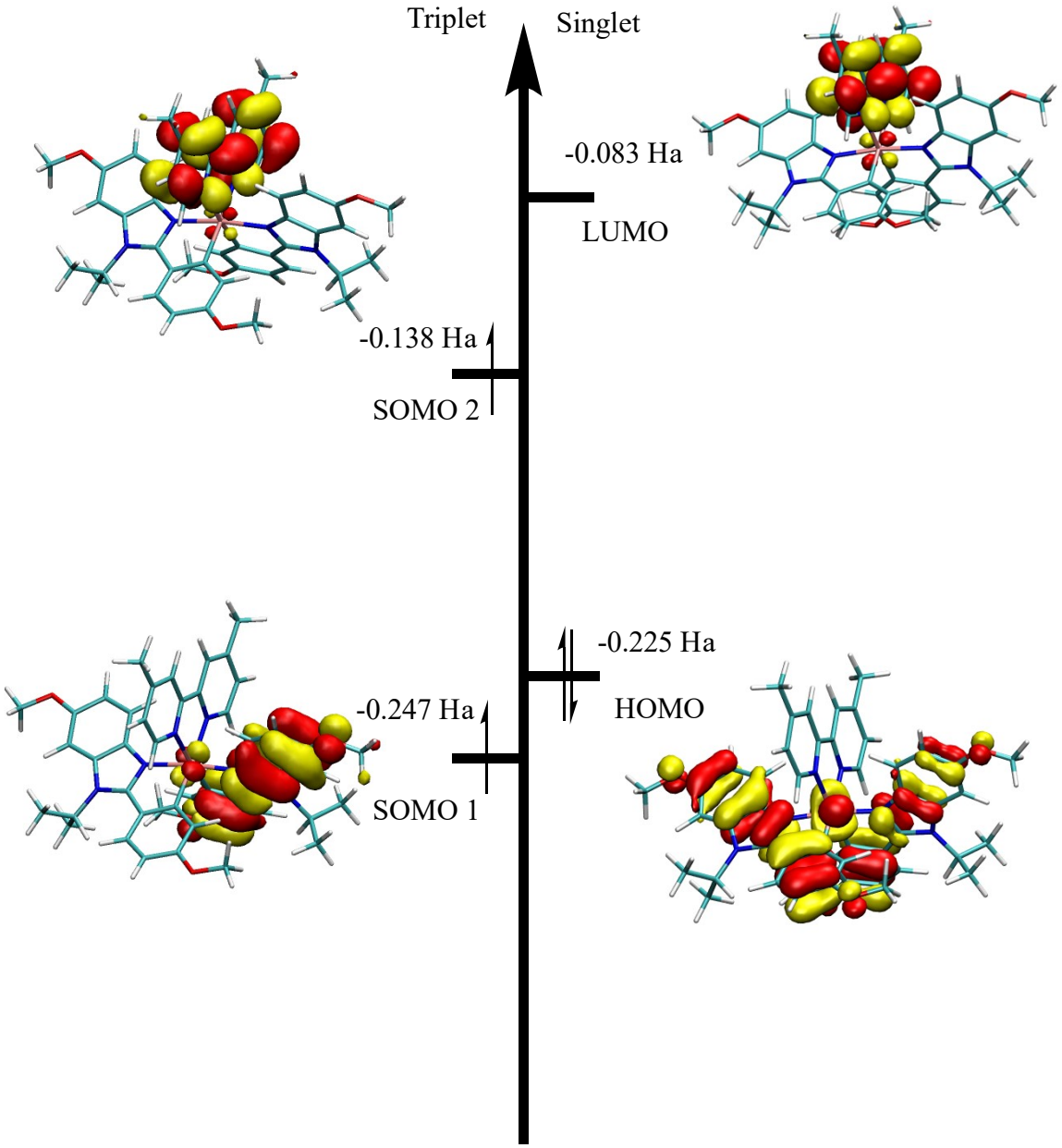

Figure S 13: Frontier orbitals of Complex **A** in the crystal: SOMO's of the triplet state (left) and HOMO/LUMO of the singlet state(right).

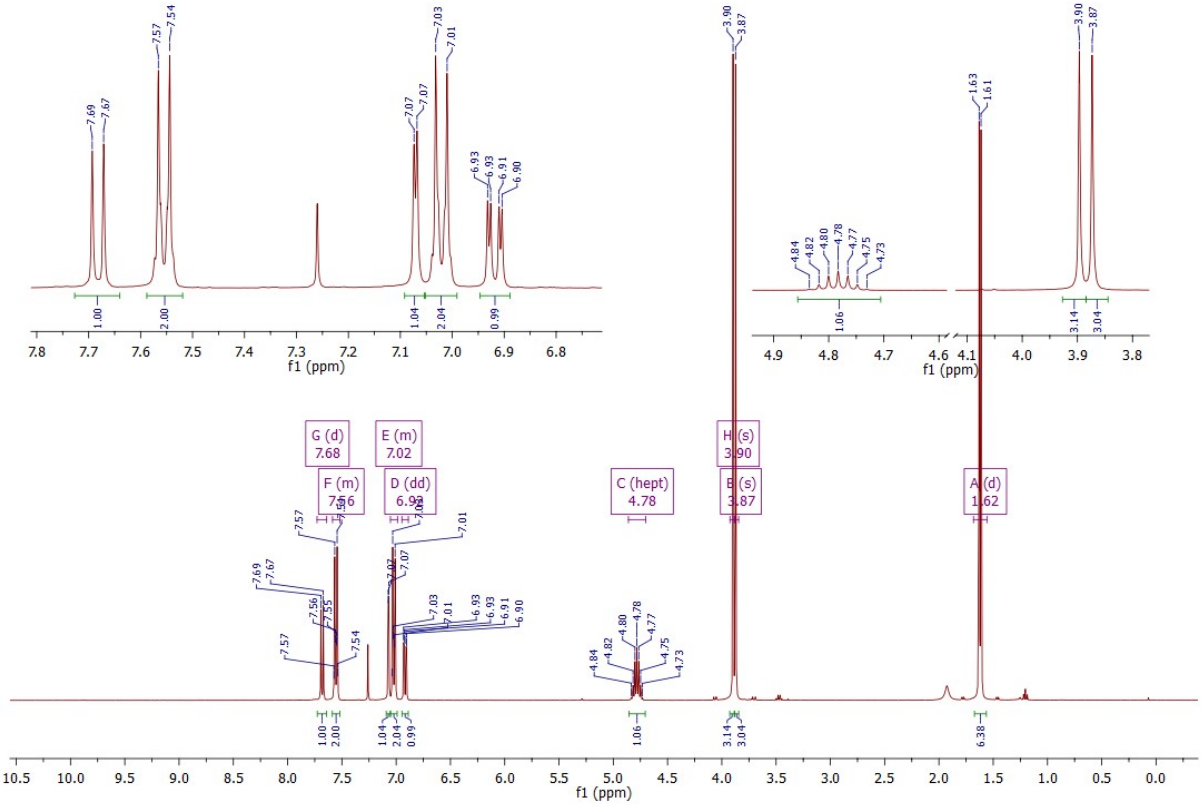

Figure S 14: ^{1}H NMR spectra of the cyclometallating ligand 400 MHz in $CDCl_3$

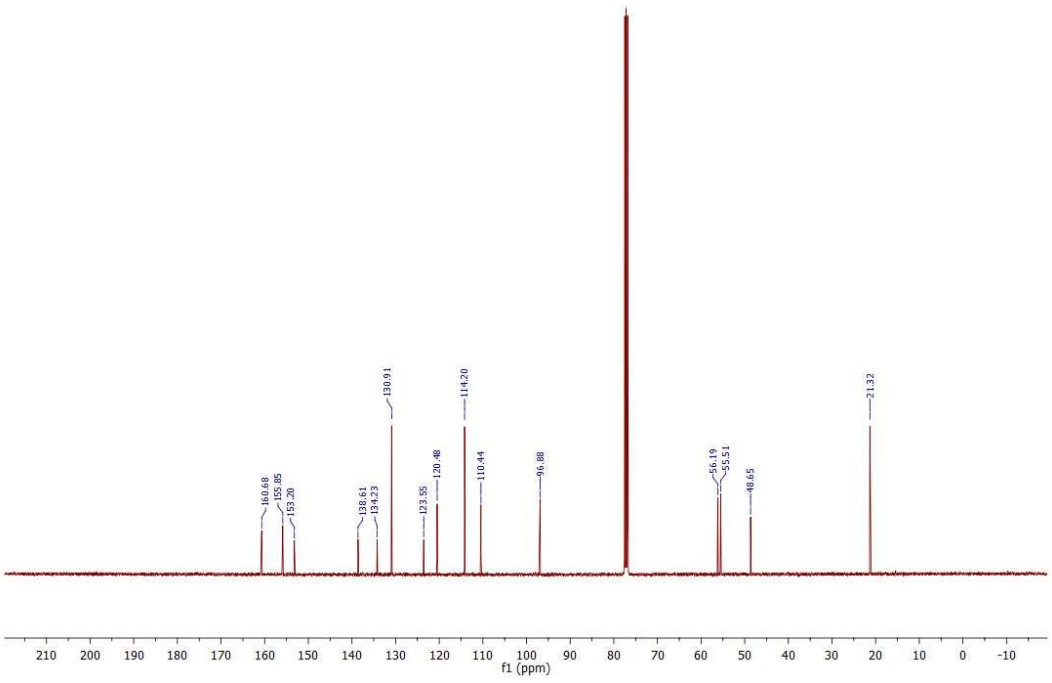

Figure S 15: ^{13}C NMR spectra of the cyclometallating ligand 101 MHz in $CDCl_3$.

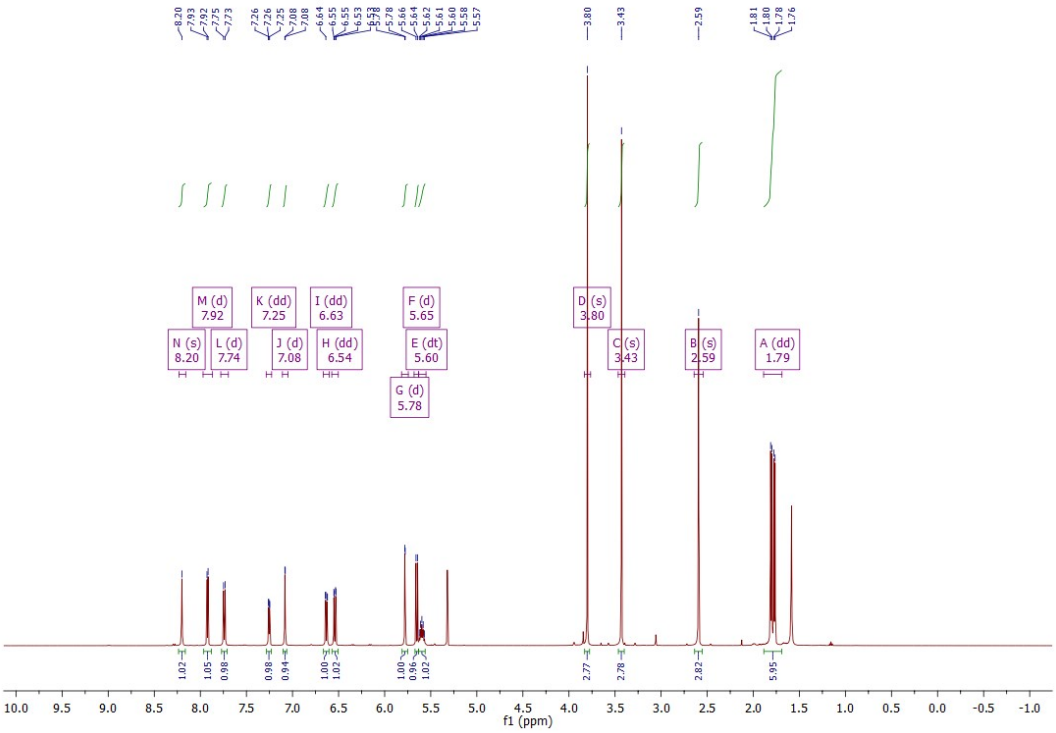

Figure S 16: ^{1}H NMR spectra of complex **A** 500 MHz in CD_2Cl_2**.**

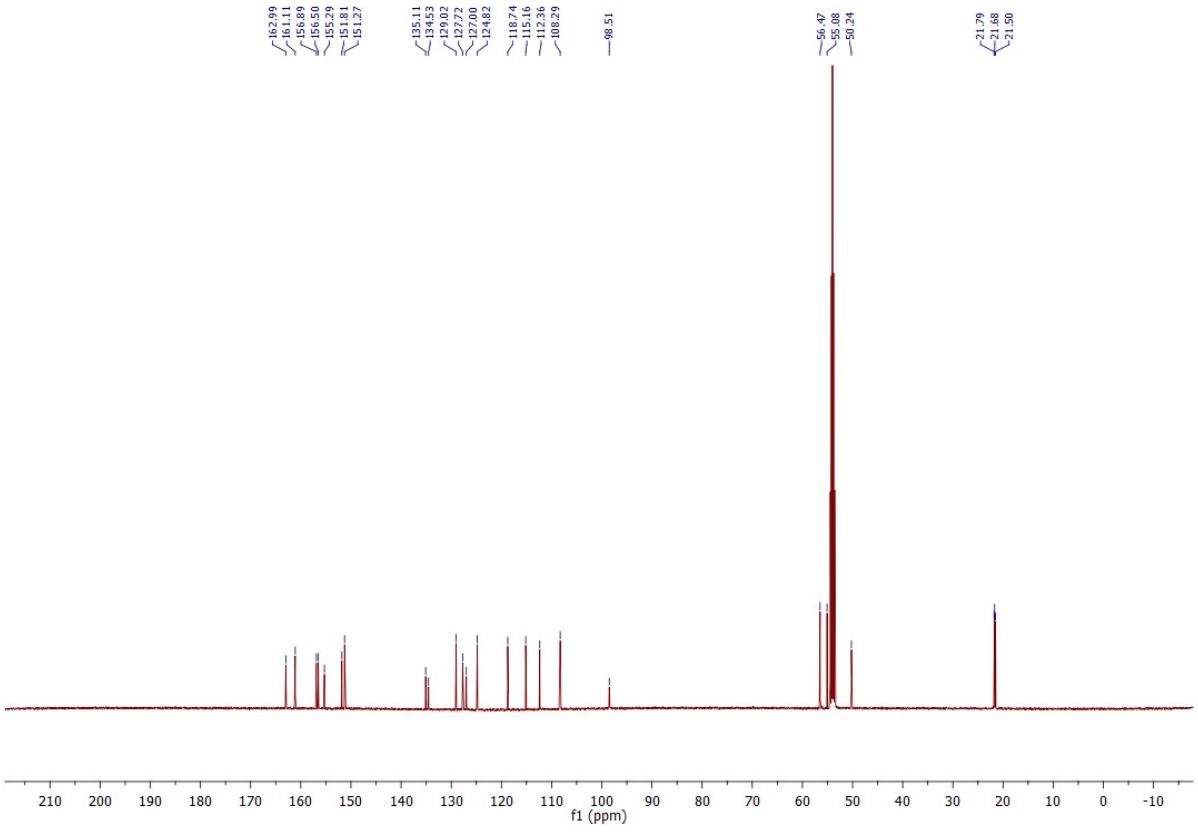

Figure S 17: ^{13}C NMR spectra of complex **A**, 126 MHz in CD_2Cl_2

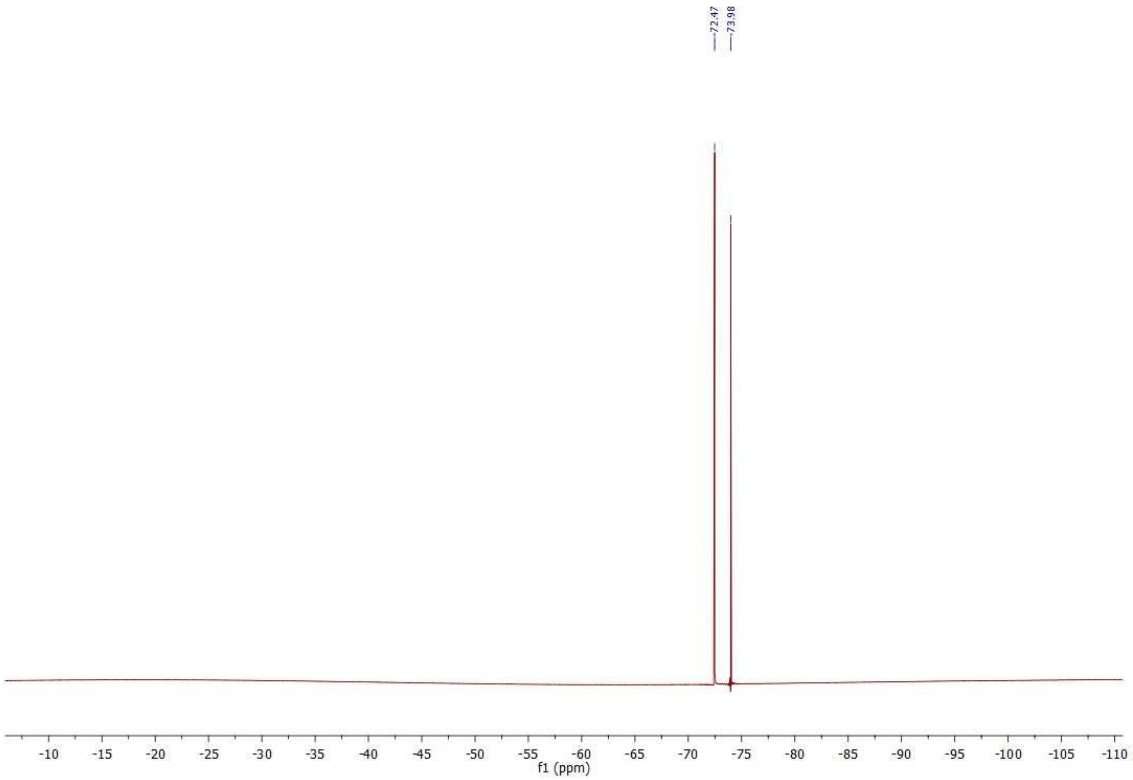

Figure S 18 : ^{19}F NMR spectra of complex **A** 470 MHz in CD_2Cl_2

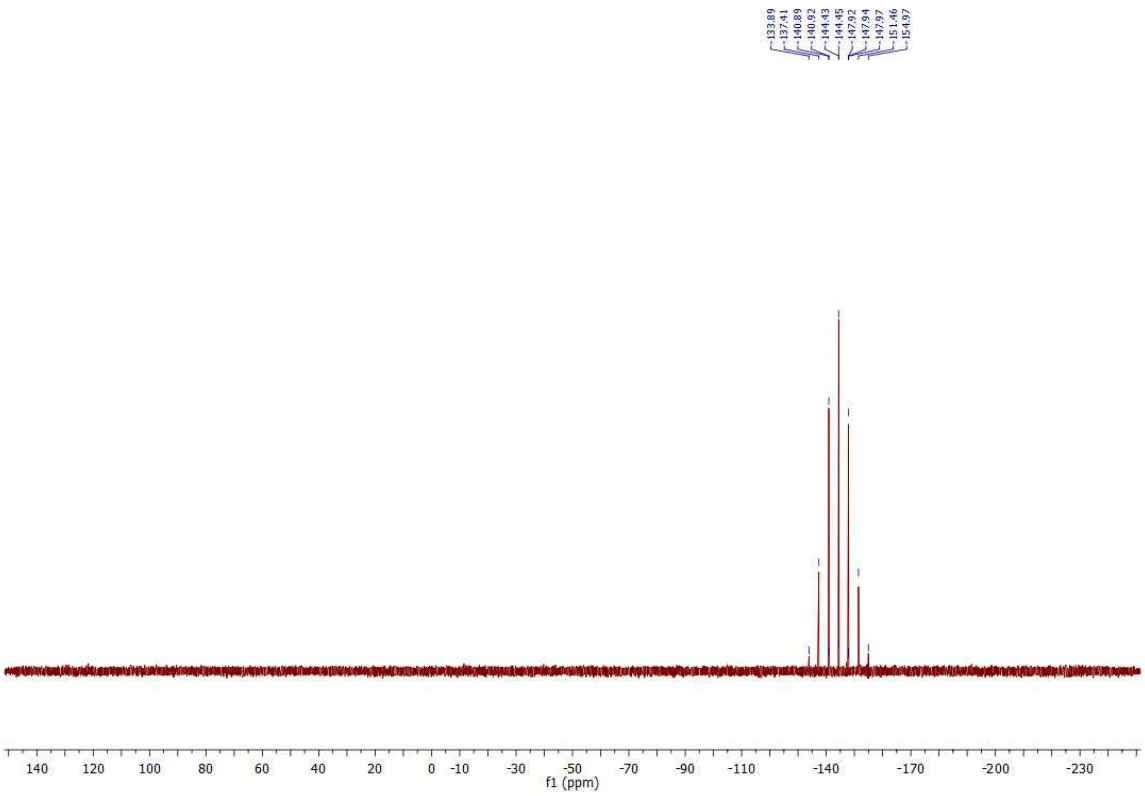

Figure S 19: ^{31}P NMR spectra of complex **A** 202 MHz in CD_2Cl_2

References

1 O. V. Dolomanov, L. J. Bourhis, R. J. Gildea, J. A. K. K. Howard and H. Puschmann, *J. Appl. Crystallogr.*, 2009, **42**, 339–341.

2 M. Nonoyama, *Bull. Chem. Soc. Jpn.*, 1974, **47**, 767.